Published in final edited form as:

Nat Cell Biol. 2009 January ; 11(1): 17–26. doi:10.1038/ncb1808.

Amoeboid T lymphocytes Require the Septin Cytoskeleton for Cortical Integrity and Persistent Motility

Aaron J. Tooley[1,*], **Julia Gilden**[1,*], **Jordan Jacobelli**[1], **Peter Beemiller**[1], **William S. Trimble**[2], **Makoto Kinoshita**[3], and **Matthew F. Krummel**[1]

[1] The Department of Pathology, University of California, San Francisco, 513 Parnassus Avenue, San Francisco, CA 94143-0511

[2] Program in Cell Biology, Hospital for Sick Children and Department of Biochemistry, University of Toronto, 555 University Avenue, Toronto, M5G 1X8, Canada

[3] Biochemistry and Cell Biology Unit, HMRO, Kyoto University Graduate School of Medicine, Yoshida Konoe, Sakyo, Kyoto 606-8501, Japan

Abstract

The systems that refine actomyosin forces during motility remain poorly understood. Septins assemble on the T cell cortex and are enriched at the mid-zone in filaments. Septin knockdown causes membrane blebbing, excess leading edge protrusions, and lengthening of the trailingedge uropod. The associated loss of rigidity permits motility, but cells become uncoordinated and poorly persistent. This also relieves a previously unrecognized restriction to migration through small pores. Pharmacologically rigidifying cells counteracts this effect, and relieving cytoskeletal rigidity synergizes with septin-depletion. These data suggest that septins tune actomyosin forces during motility, and likely regulate lymphocyte trafficking in confined tissues.

Introduction

An important feature of T lymphocytes is their migration through tissues in search of antigen presenting cells (APC) bearing peptide-MHC complexes. Both motility rate and access to tissues by T cells is highly controlled—a mechanism that is thought to be necessary to prevent accumulation in peripheral tissues and the potential breakdown of tolerance mechanisms. Motile T cells are characterized by an amoeboid ‘hand mirror’ shape in which the trailing edge pinches distinctly into a uropod. This morphology is required for efficient migration within lymph nodes and peripheral tissues, for crossing barriers to enter new tissues, and for their reactivity to antigen-bearing APC1. Their migration is characterized by actin polymerization at the leading edge ‘pseudopod’2–4, and myosin IIA-based contraction, predominantly away from the leading edge5. Some of the polarity circuits restricting leading edge extensions to the pseudopods and retraction to the uropod are likely

[4]Correspondence should be addressed to M.F.K. (email: matthew.krummel@ucsf.edu, Phone: (415) 514-3130 FAX (415) 514-3165.).

*Indicates Equal Contribution

similar to those in neutrophils6 and *Dictyostelium*7. The mechanisms that fine-tune protrusive activity and regulate the shape of the uropod, however, remain undetermined.

Septins were first identified as cell division cycle (cdc) mutants8 in yeast and assemble into concentric filaments at the mother-bud neck during cell division (reviewed in 9,10). The Septin ring around the cytokinetic furrow in yeast functions as a diffusion barrier, maintaining cell fate determinants in the appropriate cell11,12. Individual septins were independently identified in mammals on the basis of their abnormal expression in a wide range of tumors, including mammary adenocarcinomas13 and myeloid leukemias14. Additionally, the Septin 9 locus is a site of frequent retroviral insertion leading to generation of T cell lymphomas15. Since their identification in mammals, septins have been shown to play important roles in many cell types, including neurons, platelets, and spermatozoa 16–18.

Septins are cytoskeletal proteins that polymerize to form rings and gauzes19 and typically attach to the cell membrane via N-terminal phosphoinositide binding motifs. In mammals, they frequently co-localize with actin stress fibers. The mammalian septins can be divided into four groups. Filaments form from combinations of these, with members of each class potentially substituting for one another and generating a great diversity of possible arrays. A recently reported crystal structure of complexed septins indicates that the essential subunit of septin superstructures is a linear hexamer of Sept2-Sept6-Sept7 with a 2:2:2 stoichiometry20.

Here we demonstrate a critical role for Septins in T cell motility. Septins assemble along the cell cortex, enriched in an array of fibrous strands in the mid-zone. Elimination of the septin cytoskeleton using shRNA led to marked elongation of the uropod, pronounced blebbing, and excess leading edge protrusions, suggestive of uncontrolled cytoskeletal forces. While myosin II activity is required for these phenotypes, there is no evidence that actin or myosin is overactive in these cells. Rather, the motion and membrane dynamics of septin-deficient cells is consistent with a loss of membrane tension. The resulting disorganized migration of septin-deficient cells strongly suggests a corset-like function for the septin cytoskeleton, providing compression and rigidity, and supporting efficient motion of motile T cells.

Results

Septin filaments assemble on the cortex, enriched in the T cell mid-zone

We first identified T cell expression of Sept9 in a gene-trap screen21 for molecules that polarized in T cells (data not shown). Analysis of septin expression in a murine T cell line (Fig. S1A) by RT-PCR indicated expression of multiple Septins, comprising one from Group I (Septin 9), three from Group II (Septins 6,8,11), two from Group III (Septins 2 and 4) and one from Group IV (Septin 7). This RNA expression pattern is consistent with expression profiling of human septins22. Using a panel of anti-septin specific polyclonal antibodies, we also detected Septin 1,6,7,8 and 9 protein. We did not have suitable reagents to assess Sept10 expression, and other septins were not present above our level of detection (Fig. S1B and data not shown). As septins are known to form heteromeric complexes23–26, we looked for septin complexes in lysates from D10 T cells. Immunoprecipitation of Septins

1,6,7 or 9 caused co-precipitation of complexes containing the majority of Septins 1,6,7,8, and 9 respectively (Figure 1a and S5a). Although this method does not reveal the diversity of filament compositions, individual septins were clearly involved in interactions with aggregates containing every other septin.

Four anti-septin antibodies proved suitable for widefield immunofluorescence. These grossly highlighted the cell cortex in crawling T cells and were frequently enriched through the mid-zone, forming an annular septin 'corset'. This pattern was most prevalent for Septins 7 and 9 and less so for Septins 1 and 6, (Fig. 1b). More rarely and only for Sept9, we observed staining inside the cell near the MTOC (data not shown). Similar distributions were observed in primary cells (Fig. S2e)

Higher resolution confocal imaging revealed that the mid-zone distribution was highlighted by denser arrays and fibers that were partially perpendicular to the axis of travel (Fig. 1c and Movie SM1). These septin densities appear similar to the stays of a corset or sail, latitudinally-oriented features in an otherwise uniform band. Total internal reflection fluorescence microscopy (TIRF) indicated that regions of adhesion also contained these fibrous arrays (Fig 1d). Fibers are near the limit of optical resolution (≤250nm) in width and vary from short puncta to filaments longer than 3 microns. These enrichments are not simply areas of higher membrane density, as septin staining did not colocalize with membrane dyes such as DiO (Fig. S2a). In some cells, particularly for Septin6, distributions were predominantly punctate (Fig. S2b). These may represent shorter fibers, loosely connected septin structures, subcortical vesicles or another subregion of the greater septin array. Septin puncta were also the dominant distribution in rounded, non-motile T cells (Fig. S2d), suggesting a functional relationship of the Septin corset to T cell crawling. Finally, we occasionally (see Fig. 3) observed cells with excess leading-edge protrusions in wild-type T cells, and Septins, notably Septin 6, were present in these protrusions (Fig. S2c). In sum, a cortical array of septins decorates the surface of T lymphocytes.

Global Morphological and Cortical Defects in the Absence of Septins

To assess the function of septins in T cells, we targeted Septins 1, 6, 7 and 9 using plasmid-based short hairpin RNAs (shRNAs). We achieved significant knock-down (KD) of these Septins in D10 T cells when each was specifically targeted (Fig. 2a and S5b). In addition, targeting of Sept7 eliminated the entire septin complex (Fig. 2a, b). This result was specific to Sept7, as the reciprocal was not observed when other septins were targeted, supporting the hypothesis that Sept7 is critical to septin assembly 23–25,27.

To confirm that these results were specific to Sept7KD, we generated another shRNA targeting Sept7 (KD #2) at a distinct site. Expression of either shRNA resulted in similar reductions in all septins (Fig. 2b). We reproducibly achieved greater than 80% KD of Septins 6,7,8, and 9, and over 70% of Sept1 using either shRNA. Although septin knockdown causes cell division defects in other systems 26–28, Sept7KD in D10 T cells did not show such defects during the 72 hour period in which our observations were made (Fig. S3a).

While there was no apparent phenotype of individual Septin 1, 6, or 9 deficiencies, the Sept7KD-induced loss of all septins caused profound disruption in cellular morphology and motility. The most obvious morphological disruption was in cell length (Figure 2c and d). The average uropod length in KD cells was 14.4 ± 4.3 μm for Sept7KD#1 (n = 107) and 15.1 ±3.7 μm for Sept7KD #2 (n = 108) versus 8.8 ±2.0 μm for control shRNA treated cells (n = 97). In contrast cell body length was unchanged in Sept7KD cells (Fig. 2e), showing that Septins were not globally controlling cell size but were particularly necessary to regulate the mid-zone/uropod. The phenotype was independent of adhesion, as cells floating in suspension were also elongated (data not shown).

The long uropods of Sept7KD cells also frequently appeared bent (Fig. 2c, d and f). This was observed in 32% of Sept7KD#1 (n=107) and 34% of Sept7KD#2 (n=108) cells, but only 10% of control cells (n=97). This further suggests a stabilizing role for septins in maintaining and coordinating the morphology of motile cells.

Defects due to septin disruption were not confined to the uropod and also suggested poor structural integrity of the cortex. By analyzing time-lapse images (Fig. 3a and Movies SM2, SM3 and SM4), we quantified two defects in the leading edge region: membrane blebbing and excess protrusions, both of which were uncommon in wild-type T cells. As shown in Figure 3a, membrane blebbing was very dynamic and mainly confined to the cell body. Blebbing was observed in 29.7% (KD #1, n = 118) and 37.1% (KD #2, n = 140) of Sept7KD T cells versus 9.9% of the control sample (n = 151) (Fig. 3b). As visible in Figure 3a and movie SM3, cells frequently blebbed during pauses in motility, perhaps due to poor coordination of compression and elongation. Though blebbing is often associated with apoptosis, Sept7KD and control cells had similar Annexin V staining (Fig. S3b), suggesting that blebs associated with septin-deficiency arose through another pathway. Time-lapse analysis also demonstrated the formation of long, thin appendages that emanated from both the leading edge and the mid-zone in Sept7KD cells before eventually being re-absorbed. Although these protrusions occurred less frequently than membrane blebbing (Fig. 3b), there were significantly more excess protrusions in Sept7KD T cells (KD #1 = 9.3%, KD #2 = 15.0%) than in the control treated population (2.0%).

Normal Tubulin and Actin Cytoskeletal Activities in the Absence of Septins

Since many of the defects in Sept7KD cells resemble those of an overactive cytoskeleton, we analyzed the localization and activity of a complement of tubulin and actomyosin-related proteins. Tubulin and pericentrin staining were grossly normal in Sept7KD cells, though bundled microtubules were elongated through their uropods (Fig. 4a). Staining for pericentrin revealed normal positioning of the microtubule-organizing center (MTOC), directly behind the nucleus (Fig. 4b). These data indicate that the Sept7KD phenotype was not due to disorganization of microtubules.

Though an overactive actomyosin cytoskeleton could cause the blebbing, elongation and protrusions observed in septin-deficient T cells, we observed a 10% to 30% reduction in the levels of F-actin in septin-deficient cells, as assessed by phalloidin staining (Fig. 4c), which was not due to changes in total actin protein level (Fig. 4e and S5c). Phalloidin staining of T cells was grossly normal, with polymerized actin lining the cortex and mildly enriched at the

mid-zone in both control and Sept7KD cells (Fig. 4d). There were also no detectable differences in the phosphorylation state of myosin light chain (MLC) or myosin heavy chain IIA (Myh9) or changes in the overall levels of myosin II in Sept7KD cells (Fig. 4e and S5c). Likewise, in both control and Sept7KD cells, phospho-MLC staining was uniformly distributed, and mildly enriched in the cell body relative to the uropod (Fig. 4f). We would have expected additional enrichment of phospho-MLC in the mid-zone/uropod if Septins directly regulated MLC activity there. Despite these results, the blebbing, elongation and protrusions of Sept7KD cells strongly required myosin II activity. Treatment of Sept7KD and control cells with the myosin II inhibitor Blebbistatin or a Rho Kinase inhibitor Y-27632, essential for MLC activity in the uropod, resulted in complete loss of the uropod and existing blebs (Fig. 4g and 4h, and Movies SM5-SM6).

Defective Motility in the Absence of Septins

Sept7KD T cells exhibited reduced instantaneous crawling velocities *in vitro* (Fig. 5a). Sept7KD T cells crawled 7.5 ±1.9 μm/min (KD #1, n = 36) and 7.0 ±1.8 μm/min (KD #2, n = 35) compared to 8.5 ±2.6 μm/min for control cells (n = 30). More significantly, they had shorter net displacements than control cells (Control: 15.0 ± 6.1μm/min$^{1/2}$, KD #1:10.81 ± 5.8 μm/min$^{1/2}$, KD #2: 10.85 ± 4.5 μm/min$^{1/2}$). This result is surprising with respect to the findings of Figure 4 and demonstrate that despite functional actomyosin contraction, septin-deficient cells lack normal processivity. These defects were not due to decreased integrin binding by Sept7KD cells (Fig. S4a) and primary Sept7KD T cells exhibited similar defects under shear flow conditions (Fig. S4b). Since Sept7KD cells were more protrusive overall than control cells, we wondered whether Sept7KD cells were making non-productive protrusions outside the direction of motility that impeded their processivity. To address this, we measured the volume of motile cells that extended outside the path of motility and, therefore, did not propel the cell forward. We labeled the nuclei of GFP-transfected cells with Hoechst 33342 and acquired confocal three-dimensional time-lapses of crawling cells. We then created volumes representing the paths occupied by the nuclei during 15-minute movies (Fig. 5c, blue), showing the overall directions of the cells. The GFP volumes were overlaid on the nuclear path volumes at each time point and the total volumes (Fig. 5c, red outline) and the volumes extending outside the nuclear path were measured (Fig. 5c, green). The total volumes of control and Sept7KD cells were similar, but on average Sept7KD cells had about 1.5 times the extra-nuclear path volume of control cells (median volumes of 167.8 μm^3 and 249.5 μm^3 for control and Sept7KD, respectively), supporting the hypothesis that their excess protrusions do not contribute to processive motion and, therefore, contribute to diminshed motility in Sept7KD cells.

Enhanced Transmigration in the Absence of Septins

Although specific chemotaxis of D10 cells to MIP-1α is poor, control and Sept7KD T cells responded equivalently to this chemokine (Fig. 5d). However, Sept7KD exhibited two-fold higher transmigration than control cells through 8 μm pores in the absence of chemokine. Since increased motility cannot account for this greater background transmigration (Fig. 5a), we hypothesized that these cells passed through the pores, which are similar in dimension to the cells girth, more efficiently than control cells. When we challenged the cells with transwell pores considerably smaller (3 μm and 5μm) than their smallest dimension, control

treated D10 cells were essentially unable to pass through the small pores (2.0% and 3.7% migration, respectively). However, Sept7KD cells migrated through 3 and 5 μm pores approximately fivefold better than control cells (Sept7KD#1: 10.7% and 15.7% migration, respectively and, Sept7KD#2: 8.8% and 14.1% migration, respectively) and comparably to wild-type cells facing nearly 7× larger openings (Fig. 5e). This shows that septins restrict chemokine-independent migration and suggests a cell-intrinsic barrier function of the septin cytoskeleton for cells encountering small junctions.

Because D10 T cells exhibit little specific chemotaxis, we expressed a Septin7 shRNA in primary T cell blasts, which are more suitable to chemotaxis assays. With knockdown, these cells adopted the same extended-uropod phenotype as septin-deficient D10 cells (Fig. 5f.) In a chemotaxis assay using 5 μm pores, we found that septin-deficient primary cells transmigrated at a rate double that of control cells (Fig. 5f). This was accompanied by a small increase in their transmigration in the absence of chemokine.

Transmigration Efficiency is Correlated with Cortical Rigidity

Because of the extreme compression of large cells migrating through small pores, we hypothesized that a loss of cortical rigidity in septin-deficient cells allowed them to transmigrate more efficiently. To investigate this possibility, we sought to pharmacologically mimic or counteract the septin-based loss of rigidity. We treated D10 cells with nocodazole to inhibit microtubule polymerization and relax the cell cortex or with taxol to stabilize microtubules and rigidify the cortex. Interestingly, taxol treatment has previously been shown to increase cell-permeation of collagen gels29. After nocodazole treatment, both control and Sept7KD cells maintained their uropods, but appeared less compact and often generated multiple leading edges (Fig. 6a.) Conversely, when treated with taxol, both groups had few protrusions, and most became rounded (Fig. 6a, b.)

Time-lapse images of nocodazole-treated cells indicated that they exhibit a similar protrusive phenotype to Sept7KD cells. While control cells generally made one or two small protrusions in a 10-minute period, Sept7KD and nocodazole-treated cells frequently made four or five (Fig. 6c), and the persistence of each protrusion was significantly longer for Sept7KD and nocodazole-treated than control cells (Fig. 6e). Like Sept7KD cells, protrusions in nocodazole-treated cells were uncoupled from the processive motion of the cell. While protrusions frequently arose at the leading edge, their growth was not restricted to that region and they extended without adhesion in many directions, sometimes reaching so far back before being retracted that the uropod of the cell took on a forked appearance (Fig. 6f). On average, these protrusions did not extended farther from the cell body than the less frequent protrusions in control cells, though occasionally, very long (>15 μm) protrusions arose from Sept7KD and nocodazole-treated cells, but not control cells (Fig. 6d). Additionally, the means shown in Figure 6d may underestimate the true population means for Sept7 KD and nocodazole-treated cells because the most severely abnormal protrusions often extended out of the imaging plane, excluding them from this analysis.

Since the cortical phenotype after nocodazole treatment was like that of SeptKD cells, we compared the migration of Sept7KD and nocodazole or taxol-treated D10 cells through 3 μm transwell pores in the absence of chemokine (Fig. 6g). Interestingly, nocodazole-treated

control D10 cells transmigrated comparably to untreated Sept7KD cells (8.2 ± 0.7% versus 11.8 ± 0.3% and 12.5 ± 1.8% for KD #1 and KD #2, respectively) while few (1.9 ± 0.1%) control cells migrated. When Sept7KD cells were treated with nocodazole, the effect was greater than additive, with (35.1 ± 1.9% of KD #1 and 30.9 ± 7.7% of KD #2 cells). Conversely, when cells were stiffened with taxol, less than 1.5% passed through the pores, even among Sept7KDs. These data support the hypothesis that septin depletion relaxes the cell cortex, allowing highly efficient movement through spaces much smaller than the resting cell diameter.

Discussion

Given the many phenotypic abnormalities of septin-deficient cells, septin filaments, being cortically enriched and punctuated by occasional fibers and puncta, may function as a molecular corset. A thin and uniform septin network prevents blebs at the leading edge where actin and myosin are highly dynamic30. We hypothesize that the dynamic turnover of actomyosin filaments and their short length may be complemented by the stays of long septin filaments which are probably stable over time31,32. This stability may provide background rigidity against which global and local actomyosin forces are applied.

This fine-tuning of forces is clearly evident in movies of septin-deficient cells; septin loss has a profound effect on coordinated crawling and processivity of D10 cells. We propose that in highly dynamic amoeboid cells, it may be critical to contain and direct forces generated over their short lengths. At cellular lengths of 5–15 μm, compression forces would tend to propagate across the entire cytoplasm very rapidly33 and could generate inefficient motility if translated into bulk movements that did not reflect the required directionality. It is therefore interesting to note that foraging *Dictyostelium* lack septins and that their response to chemotactic stimuli, unlike that of T cells, is characterized by increased production of blebs and excess protrusions in multiple directions. Large numbers of protrusions extending in many directions may allow cells to better survey their environments, and *Dictyostelium* have evolved to select certain protrusions, rather than restrict their initial number34.

The cortical instability of septin-deficient cells may be related to their enhanced capacity for migration across small openings. Transwell migration assays assume cells are not able to cross a barrier with dimensions smaller than the cell's resting girth in the absence of a motive force. We found that this is not the case in the absence of septins. At present, it is unclear whether septin-dependent repression of basal migration is due to additional leading edges (septin-deficient cells find holes more easily) or the loss of cortical stability (septin-deficient cells are more deformable). Although our experiments with nocodazole treatment do not directly distinguish between those possibilities, that cortical stabilization by taxol treatment inhibits transmigration suggests that the relative fluidity of Sept7KD cells allows them to pass readily through small pores. Since T cell nuclei are typically larger than 3μm in diameter, septins may also regulate nuclear shape—indeed septins interact with anillin, which, prior to cell division is associated with the nuclear envelope35.

These observations may have important implications for *in vivo* transmigration and tumor metastasis. Cells entering or exiting tissues must squeeze through or between endothelial

cells; loss of a basal restriction on this may contribute to metastatic proficiency. Since septin expression is frequently altered in human and mouse tumors22,36,37 and Sept2 (Diff6) was first identified as an over-expressed gene in a tumor line selected for metastasis38, we speculate that destabilization of the cell cortex due to stoichiometric changes in septin complexes may facilitate tumor metastasis and progression.

Methods

Cell Culture

The D10.G4 CD4+ T cell clone was used in all experiments and was maintained in RPMI 1640 supplemented with 10% FCS, L-glutamine, penicillin, streptomycin, β-mercaptoethanol and 50 U/ml interleukin-2 (IL-2) as described5. Cells were re-stimulated weekly with conalbumin (134–146) peptide-pulsed irradiated splenocytes from B10.BR donor mice. Primary T cell blasts were generated by stimulating lymph node and spleen cells from DO11.10 TCR transgenic mice *in vitro* with 1 μg/mL of ovalbumin (323–339) peptide. All mice were bred and maintained in accordance with the guidelines of the Lab Animal Resource Center of the University of California at San Francisco.

Antibodies and reagents

The following antibodies were used for cell staining and immunoblotting: anti-phospho-MLC2 (Ser19) mouse monoclonal #3675 (Cell Signaling); anti-actin, clone C4 (Chemicon); anti-α-tubulin clone B-5-1-2 (Sigma); anti-pThr1939-Myh9, a rabbit polyclonal made against a c-terminal phosphopeptide of Myh95; rabbit anti-class II myosin polyclonal (BTI); and rabbit polyclonal anti-pericentrin (Covance). Polyclonal anti-peptide antibodies were generated against Anti-Sept6C (C)AGGSQTLKRDKEKKN, anti-Sept7 (C)EQQNSSRTLEKNKKKGKIF, anti-Sept8 (C)+ALHATSQQPLRKDKDKKN, and anti-Sept9 (C)IHFEAYRVKRLNEG OR (C)SAMANGVEEKEPEAPEM—two sera generated similar staining and blotting results, where the additional cysteine residues, indicated in parentheses, permitted covalent coupling to Imject Maleimide Activated mcKLH (Pierce Biotechnology, Rockford, IL) for immunization and to Sulfolink beads (Pierce) for affinity purification. Anti-Sept1 antibodies were generated against a His-tagged sequence of mouse Sept1 (NM_017461) comprising the first 366 amino acids (MDKEYV-GEQSDVL) expressed in E.coli. Affinity purified antibodies did not cross react with other septins and detected the predicted band(s). For anti-peptide antibodies, these bands were eliminated if the antibody was pre-incubated with the immunization peptide (not shown). Specificity was also indicated (Fig. 2) in the specific loss of septins 1, 6, and 9 when these were targeted by shRNA.

Lysis, immunoprecipitation and immunoblotting

D10 T cells were lysed in PBS containing 1% Triton X-100 in the presence of a cocktail of protease and phosphatase inhibitors (2 μg/ml aprotinin, 2 μg/ml leupeptin, 2 mM PMSF, 10 mM sodium fluoride, 10 mM iodoacetamide and 1 mM sodium orthovanadate). Equal amounts of cell lysates, as determined with the BioRad detergent-compatible protein assay, were then resolved by SDS-PAGE, and immunoblotting analysis was performed using antibodies described above. For immunoprecipitations, both calcium and magnesium

chloride (1 μm each) were added to the lysis buffer, and septin complexes were immunoprecipitated from D10 lysates for three hours at 4 C using Protein-A sepharose beads. Lysates were pre-cleared with beads coated with normal rabbit serum.

Cell staining

Cells were incubated at 37 C on superfrost plus slides (VWR International) for at least one hour before fixing with 1% PFA (supplemented with 1 mM calcium and magnesium chloride) at 37 C for 10 min. Cells were then centrifuged onto the slides at 200×g for 5 min. Fixed cells were blocked with 2% donkey serum and permeabilized with 0.2% saponin (Sigma) in PBS for 30 min. Cells were incubated with primary antibodies for 60 min, washed, then stained with secondary antibodies for 60 min. After thorough washing, cells were treated with anti-fade reagent (BioRad), and the slides sealed and imaged. For septin staining, only polarized crawling T cells were scored for enrichment at the T cell mid-zone. All image analysis and measurements were done using Metamorph software.

Plasmids and transfectionss

shRNAs were cloned into the pSilencer 2.0 shRNA expression vector using the human U6 promoter (Ambion) following manufacturers instructions. Two hairpins were designed against Sept7 (KD #1, 5′-GGATTTGAATTCACTCTTA-3′ and KD #2, 5′-GGATCCGTTTGACCAATTT-3′), targeting the open reading frame and the 3′ untranslated region, respectively. Hairpins against Sept1 (5′-GCCTGCCCTTGCACTTAAA-3′), Sept6 (5′-GCTTAAGTCTCTGGACCTAGT-3′) and Sept9 (5′-GCCTAAGCAAAGTGGTGAACA-3′) were also used in this study. A negative control vector containing an shRNA with only limited sequence homology to any known sequence in the mouse genome (5′-ACTACCGTTGTTATAGGTG –′3) was used a negative control. Control and shRNA expressing plasmids were introduced into T cells by electroporation (Bio-Rad) and co-transfection of an EGFP expressing vector, pEGFP-N1 (Clontech), was used as a positive marker for transfection and for cell sorting. For transfection, 25 μg of plasmid DNA in a >7:1 molar ratio of shRNA expressing plasmid to GFP reporter was used to transfect 50 million cells in a 0.5 ml volume. GFP positive cells were sorted 48–72 hours post-transfection using a MoFlo cell sorter (DakoCytomation). Sorted GFP positive cells were used approximately 72 hours post-transfection in all knockdown experiments in this study.

Retroviral Infections

The Sept7 KD#1 hairpin was cloned into pSIREN-Retro-Q-ZsGreen1 (Clontech), which was then used in calcium phosphate transfection of phoenix cells. Virus-containing supernatant from these cells was used on two consecutive days (days 2 and 3 after activation) to spin-infect DO11.10 T cell blasts. Cells were sorted according to their ZsGreen expression on day 4 and rested for 24 hours before experiments were performed.

Microscopy

Imaging experiments were done using a modified ZeissAxiovert 200M microscope with a plan-neofluor 40× objective (Carl Zeiss). The microscope was fitted with dual excitation and

emission filter wheels and a Coolsnap HQ camera (Roper Scientific). Image acquisition and analysis was performed using Metamorph imaging software (Molecular Devices). To examine T cell motility *in vitro*, imaging was performed in 0.25% low-melting point agarose and time-lapse images were recorded at 5, 10 and 30 second intervals. For velocity measurements, Hoechst 33342 (1 μg/ml) was added to the imaging chamber to visualize the nucleus and time-lapse images were acquired at 30-second intervals. Migration of the nucleus was then used to track the cell path for velocity measurements. To examine membrane dynamics, time-lapse images were acquired at higher frequencies (5 and 10 second intervals).. Only cells that could be observed for at least 5 minutes were included in analysis. For extra-nuclear path volume experiments, initial frames were excluded from analysis, as most of the extranuclear volume in those images was due to the trailing uropod.

Analysis and Statistical Measures

Velocity and displacement were analyzed in Imaris (BitPlane). Image processing and measurements for extra-nuclear path volume was done in Matlab using Image Processing Toolbox functions (The Mathworks). All statistical analyses were performed in Graphpad Prism and individual tests are named in the figure legends.

Inhibitor studies

When cells were treated with the myosin II inhibitor Blebbistatin (racemic, 100 μM final) or ROCK inhibitor Y-27632 (10 μM final), 0.1% low-melting point agarose was used, since the drugs did not diffuse well in 0.25% agarose. Nocodazole and Taxol (Sigma-Aldrich) were used at 5 μM, and cells were exposed to the drugs for at least 30 minutes prior to those assays. DMSO controls did not alter the morphology or crawling of control or shRNA treated cells.

F-Actin quantification

Cells were fixed immediately after removing from 37 C to maintain cell morphology. T cells were permeabilized and stained using 3 units of Alexa Fluor 647-conjugated phalloidin according to the manufacturer's protocol (Invitrogen). F-Actin staining was quantified using a BD FacsCalibur and data was analyzed using FlowJo (TreeStar).

Transmigration assay

Transmigration assays were carried out using transwells (Corning) with 3μm, 5μm or 8μm pores in the absence of chemokine. Transmigration assays were performed at 37°C for 4 hours in the absence of FCS, before cells were harvested and counted for a fixed amount of time on a BD FACSCalibur flow cytometer. Data was analyzed using CellQuest Facs analysis software.

Supplementary Material

Refer to Web version on PubMed Central for supplementary material.

Acknowledgments

We thank A. Weiss and M.T. McManus for insight and critical discussions, ShuWei Jiang and Cliff McArthur for expert technical assistance with cell sorting and Christine Lin and Ed Shimazu for computer support. We also thank Cynthia Voong for critical reading of the manuscript and members of the Krummel lab for thoughtful discussions. This work was supported by the NIH(R21-AI062899), the Sandler family fund, the National Science Foundation, and the Leukemia and Lymphoma Society.

References

1. Sanchez-Madrid F, del Pozo MA. Leukocyte polarization in cell migration and immune interactions. Embo J. 1999; 18:501–11. [PubMed: 9927410]
2. Yan C, et al. WAVE2 deficiency reveals distinct roles in embryogenesis and Rac-mediated actin-based motility. Embo J. 2003; 22:3602–12. [PubMed: 12853475]
3. Snapper SB, et al. WASP deficiency leads to global defects of directed leukocyte migration in vitro and in vivo. J Leukoc Biol. 2005; 77:993–8. [PubMed: 15774550]
4. Snapper SB, et al. N-WASP deficiency reveals distinct pathways for cell surface projections and microbial actin-based motility. Nat Cell Biol. 2001; 3:897–904. [PubMed: 11584271]
5. Jacobelli J, Chmura SA, Buxton DB, Davis MM, Krummel MF. A Single Class II Myosin Modulates T cell Motility and Stopping But Not Synapse Assembly. Nature Immunology. 2004; 5:531–538. [PubMed: 15064761]
6. Xu J, et al. Divergent signals and cytoskeletal assemblies regulate self-organizing polarity in neutrophils. Cell. 2003; 114:201–14. [PubMed: 12887922]
7. Sasaki AT, et al. G protein-independent Ras/PI3K/F-actin circuit regulates basic cell motility. J Cell Biol. 2007; 178:185–191. [PubMed: 17635933]
8. Koshland D, Kent JC, Hartwell LH. Genetic analysis of the mitotic transmission of minichromosomes. Cell. 1985; 40:393–403. [PubMed: 3881185]
9. Versele M, Thorner J. Some assembly required: yeast septins provide the instruction manual. Trends Cell Biol. 2005; 15:414–24. [PubMed: 16009555]
10. Kinoshita M. Diversity of septin scaffolds. Curr Opin Cell Biol. 2006; 18:54–60. [PubMed: 16356703]
11. Barral Y, Mermall V, Mooseker MS, Snyder M. Compartmentalization of the cell cortex by septins is required for maintenance of cell polarity in yeast. Mol Cell. 2000; 5:841–51. [PubMed: 10882120]
12. Takizawa PA, DeRisi JL, Wilhelm JE, Vale RD. Plasma membrane compartmentalization in yeast by messenger RNA transport and a septin diffusion barrier. Science. 2000; 290:341–4. [PubMed: 11030653]
13. Montagna C, et al. The Septin 9 (MSF) gene is amplified and overexpressed in mouse mammary gland adenocarcinomas and human breast cancer cell lines. Cancer Res. 2003; 63:2179–87. [PubMed: 12727837]
14. Osaka M, Rowley JD, Zeleznik-Le NJ. MSF (MLL septin-like fusion), a fusion partner gene of MLL, in a therapy-related acute myeloid leukemia with a t(11;17)(q23;q25). Proc Natl Acad Sci U S A. 1999; 96:6428–33. [PubMed: 10339604]
15. Sorensen AB, et al. Sint1, a common integration site in SL3-3-induced T-cell lymphomas, harbors a putative proto-oncogene with homology to the septin gene family. J Virol. 2000; 74:2161–8. [PubMed: 10666245]
16. Ihara M, et al. Cortical organization by the septin cytoskeleton is essential for structural and mechanical integrity of mammalian spermatozoa. Dev Cell. 2005; 8:343–52. [PubMed: 15737930]
17. Tada T, et al. Role of Septin cytoskeleton in spine morphogenesis and dendrite development in neurons. Curr Biol. 2007; 17:1752–8. [PubMed: 17935993]
18. Dent J, et al. A prototypic platelet septin and its participation in secretion. Proc Natl Acad Sci U S A. 2002; 99:3064–9. [PubMed: 11880646]
19. Rodal AA, Kozubowski L, Goode BL, Drubin DG, Hartwig JH. Actin and septin ultrastructures at the budding yeast cell cortex. Mol Biol Cell. 2005; 16:372–84. [PubMed: 15525671]

20. Sirajuddin M, et al. Structural insight into filament formation by mammalian septins. Nature. 2007; 449:311–5. [PubMed: 17637674]
21. Tooley AJ, Jacobelli J, Moldovan MC, Douglas A, Krummel MF. T cell synapse assembly: proteins, motors and the underlying cell biology. Semin Immunol. 2005; 17:65–75. [PubMed: 15582489]
22. Hall PA, Jung K, Hillan KJ, Russell SE. Expression profiling the human septin gene family. J Pathol. 2005; 206:269–78. [PubMed: 15915442]
23. Kinoshita M, Field CM, Coughlin ML, Straight AF, Mitchison TJ. Self-and actin-templated assembly of Mammalian septins. Dev Cell. 2002; 3:791–802. [PubMed: 12479805]
24. Kremer BE, Haystead T, Macara IG. Mammalian septins regulate microtubule stability through interaction with the microtubule-binding protein MAP4. Mol Biol Cell. 2005; 16:4648–59. [PubMed: 16093351]
25. Nagata K, Asano T, Nozawa Y, Inagaki M. Biochemical and cell biological analyses of a mammalian septin complex, Sept7/9b/11. J Biol Chem. 2004; 279:55895–904. [PubMed: 15485874]
26. Surka MC, Tsang CW, Trimble WS. The mammalian septin MSF localizes with microtubules and is required for completion of cytokinesis. Mol Biol Cell. 2002; 13:3532–45. [PubMed: 12388755]
27. Spiliotis ET, Kinoshita M, Nelson WJ. A mitotic septin scaffold required for Mammalian chromosome congression and segregation. Science. 2005; 307:1781–5. [PubMed: 15774761]
28. Nagata K, et al. Filament formation of MSF-A, a mammalian septin, in human mammary epithelial cells depends on interactions with microtubules. J Biol Chem. 2003; 278:18538–43. [PubMed: 12626509]
29. Ratner S, Sherrod WS, Lichlyter D. Microtubule retraction into the uropod and its role in T cell polarization and motility. J Immunol. 1997; 159:1063–7. [PubMed: 9233597]
30. Ponti A, Machacek M, Gupton SL, Waterman-Storer CM, Danuser G. Two distinct actin networks drive the protrusion of migrating cells. Science. 2004; 305:1782–6. [PubMed: 15375270]
31. Caviston JP, Longtine M, Pringle JR, Bi E. The role of Cdc42p GTPase-activating proteins in assembly of the septin ring in yeast. Mol Biol Cell. 2003; 14:4051–66. [PubMed: 14517318]
32. Dobbelaere J, Gentry MS, Hallberg RL, Barral Y. Phosphorylation-dependent regulation of septin dynamics during the cell cycle. Dev Cell. 2003; 4:345–57. [PubMed: 12636916]
33. Charras GT, Yarrow JC, Horton MA, Mahadevan L, Mitchison TJ. Non-equilibration of hydrostatic pressure in blebbing cells. Nature. 2005; 435:365–9. [PubMed: 15902261]
34. Andrew N, Insall RH. Chemotaxis in shallow gradients is mediated independently of PtdIns 3-kinase by biased choices between random protrusions. Nat Cell Biol. 2007; 9:193–200. [PubMed: 17220879]
35. Field CM, Coughlin M, Doberstein S, Marty T, Sullivan W. Characterization of anillin mutants reveals essential roles in septin localization and plasma membrane integrity. Development. 2005; 132:2849–60. [PubMed: 15930114]
36. Russell SE, Hall PA. Do septins have a role in cancer? Br J Cancer. 2005; 93:499–503. [PubMed: 16136025]
37. Hall PA, Russell SE. The pathobiology of the septin gene family. J Pathol. 2004; 204:489–505. [PubMed: 15495264]
38. Nottenburg C, Gallatin WM, St John T. Lymphocyte HEV adhesion variants differ in the expression of multiple gene sequences. Gene. 1990; 95:279–84. [PubMed: 2174398]

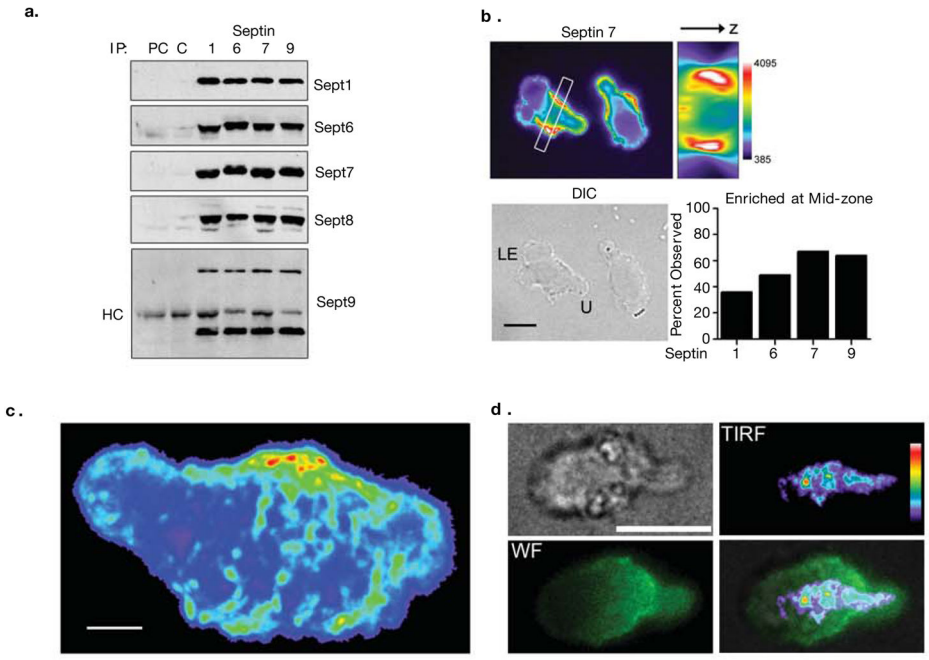

Figure 1. Septin Complexes form in T cells, assemble on the cortex and form filaments and puncta in the mid-zone

(**a**) Septins form heteromeric complexes in D10 T cells. Septins 1, 6, 7 or 9 were immunoprecipitated from D10 lysate and blotted for expressed septins. Normal rabbit serum was used to pre-clear (PC) the lysate and as a control for the immunoprecipitation (C). The band present in all samples in the Sept9 blot corresponds to the heavy chain (HC) of the antibody used for the immunoprecipitation. (**b**) Septins localize to the cell cortex in crawling D10 T cells and are frequently enriched in the mid-zone. Crawling D10 T cells were fixed and stained for Septins 1, 6, 7 (shown) and 9 (anti-Sept8 antibodies did not reproducibly stain fixed cells) and the portion of samples with significant enrichment at the mid-zone was quantified by blind-scoring Sept7 (n = 67), Sept9 (n = 64), Sept1 (n = 66), Sept6 (n=68). A three-dimensional reconstruction of a transverse section (indicated by the white box), demonstrating the presence of an annular Sept7 collar at the T cell mid-zone. Bar, 10 μm, LE = leading edge, U = uropod. Pooled totals from three independent experiments. (**c**) Confocal images of anti-Sept7 staining were acquired, and a maximum intensity projection was compiled. Distinct punctate and fibrous regions of Sept7 are found in the T cell mid-zone and uropod, indicating the presence of septin filaments. All are at or near the cortex (2 others are shown in supplemental Movie SM1). **(d)** Composite TIRF and wide-field imaging also demonstrates that fibrous Septin7 is at or near the coverslip surface. Cells were stained with anti-Septin7 and illuminated by TIRF (shown as pseudocolor) or widefield (shown as green) illumination. Scale bars in c and d are 3 and 10 μm, respectively.

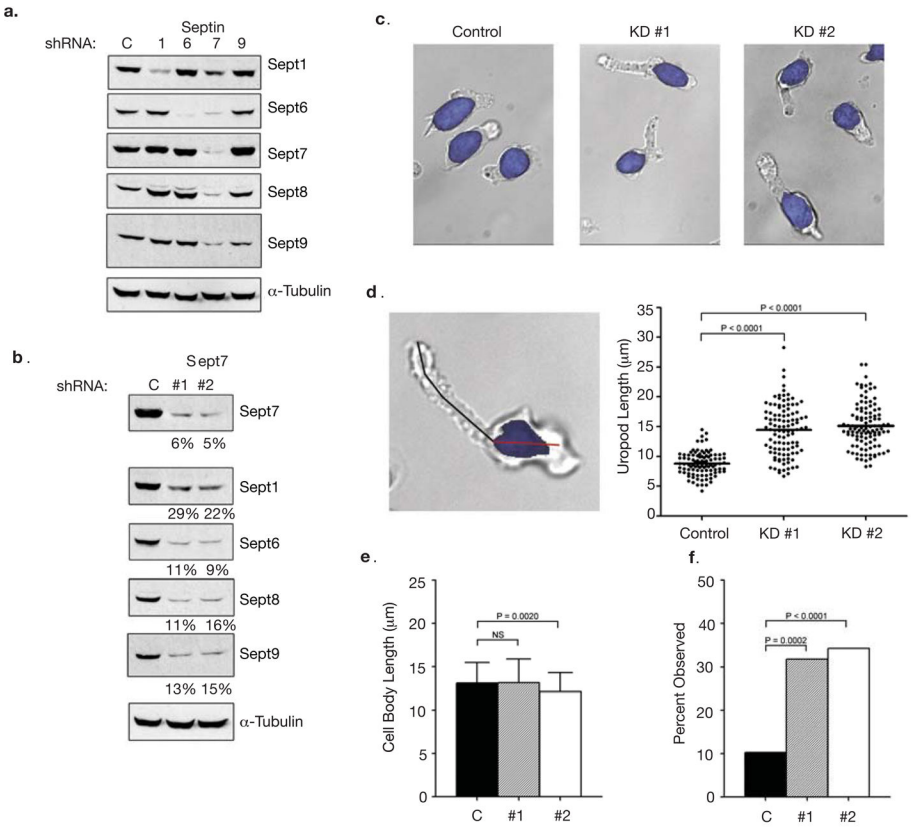

Figure 2. Septin knock-down in T cells results in augmented length and bending of uropods

(**a**) Individual shRNAs against Septins 1, 6, 7, 9 and a negative control shRNA (C = control) were transfected into D10 T cells. Protein levels were examined by Western blotting 72 hours post-transfection. KD of Sept7 results in the loss of all other known septins. For Sept9, only the predominant 40 kD isoform is shown; however, the larger isoforms are reduced as well (data not shown). This result confirms the specificity of the antibodies used throughout this study. (**b**) Reduction in septin complexes is specific to Sept7. A second shRNA at a distinct location was generated to confirm the results were specific to targeting Sept7. (**c**) Sept7KD D10 T cells have morphological defects as exhibited by an increase in uropod length. Hoechst 33342 was used to distinguish the nucleus (highlighted in blue) from the cytoplasm. (**d**) Increased uropod length in Sept7KD T cells. A line was drawn from the end of the uropod to the nucleus (black line). Sept7KD#1 (n = 107), Sept7KD#2 (n = 108) and control shRNA treated cells (n = 97). (**e**) Normal cell body length in Sept7KD T cells, measured as in **d** for cell body region (red line in d). (**f**) Bent uropods in the absence of septin complexes. A uropod was scored as bent if a straight line could not be drawn through the cell from the distal tip of the uropod to the beginning of the nucleus. KD #1, n = 107, KD #2, n = 108 and shRNA control cells, n = 97). (**d**, **e**) Representative mean ± standard deviation pooled from three independent experiments. Statistical analysis performed using a Kruskal-Wallis test with Dunn's post-test. (**f**) Pooled total from three independent experiments, statistical analysis performed using the chi-squared test.

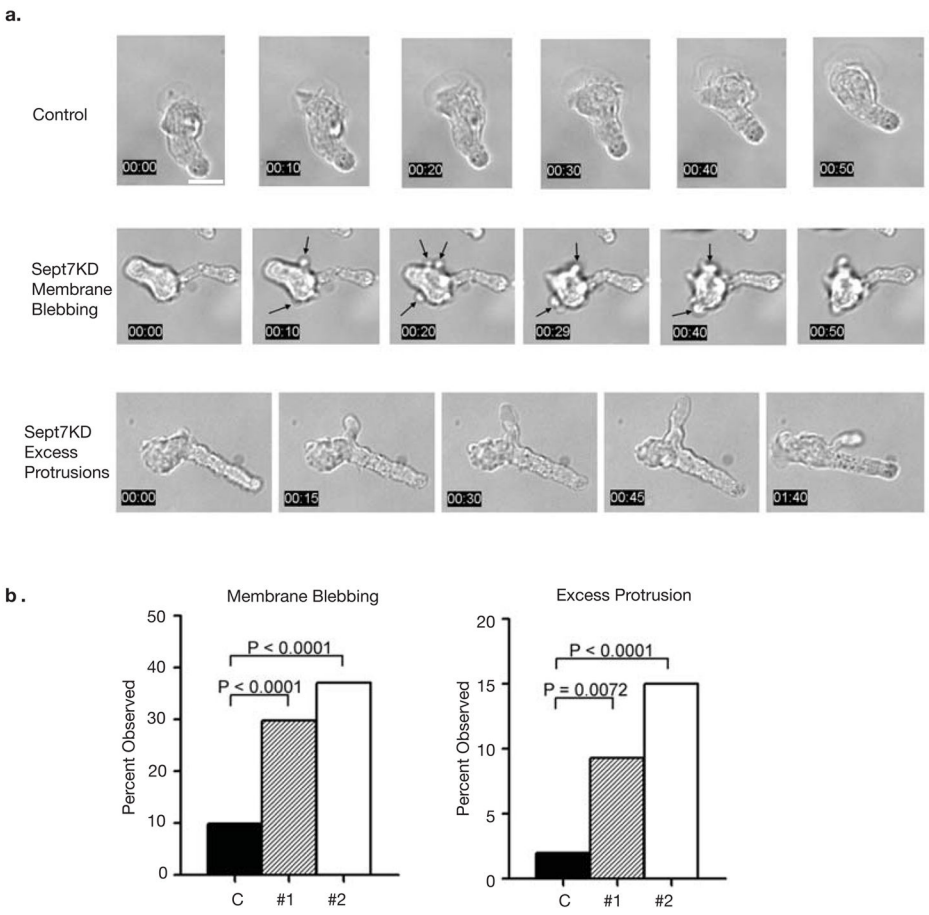

Figure 3. Septin complexes are required for structural stability of the cell cortex and at the T cell mid-zone

(**a**) Sept7KD T cells have structural defects resulting in membrane blebbing and excess membrane protrusions (also see Supplementary movies SM2, SM3 and SM4). Membrane blebbing was dynamic and mainly confined to the cell body. Excess protrusions emanated from both the leading edge and the T cell mid-zone and persisted as long, thin membrane appendages that were eventually re-absorbed in the mid-zone/rear. Scale bar represents 10 μm (**b**) Quantification of structural defects observed in Sept7KD T cells. Pooled totals from three independent experiments. Statistical analysis performed using the chi-squared test.

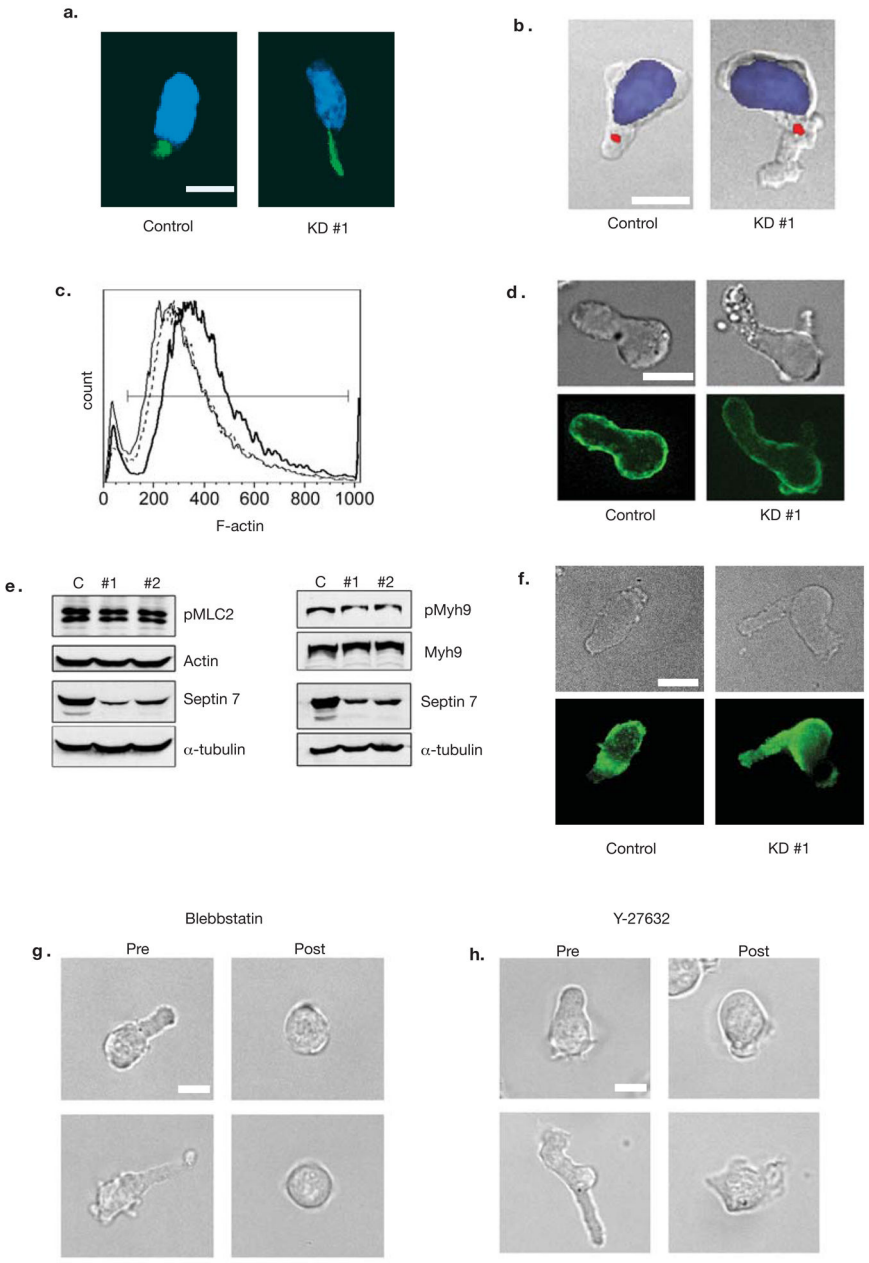

Figure 4. Integrity of Tubulin and Actomyosin Cytoskeletons in Septin-deficient T cells

The tubulin cytoskeleton was assessed using DAPI (blue) and anti-tubulin (green) (**a**) or anti-pericentrin (red) **(b)** antibodies in control and Sept7KD cells. The pericentrin-containing MTOC (red) was correctly positioned behind the nucleus (DAPI, blue) in greater than 97% of both control and septin deficient cells with at least 34 cells scored. **(c)** FACS analysis of phalloidin staining. F-actin levels were slightly reduced in Septin-deficient cells. (control = bold line, KD #1 = solid line, KD #2 = dotted line). Levels of total actin were not altered in these cells (shown in **e**). Similar results were obtained in three independent experiments **(d)** Overall distribution of actin as assessed by immunofluorescence was cortical for both control and Sept7KD cells. (**e**) Myosin II was not over-active in Sept7KD T

cells. Lysates from control or Sept7KD cells were assessed by Western blotting for the phosphorylation of the myosin light chain (pMLC2 Ser19) and heavy chain (pMyh9). **(f)** Staining for phospho-MLC(Ser19). Active Myosin light-chain kinase was not overabundant in the mid-zone in Sept7KD cells. **(g, h**) Treatment of cells with the myosin II inhibitor Blebbistatin or with the ROCK inhibitor Y-27632 resulted in T cell rounding and loss of blebs, indicating these molecules were still required for uropod formation in the absence of septin complexes. T cell rounding was observed in greater than 95% of cells scored for both inhibitors, with at least 84 cells scored from three independent experiments. Results were similar for Sept7 KD #2 (data not shown). Scale bars represent 10 μm.

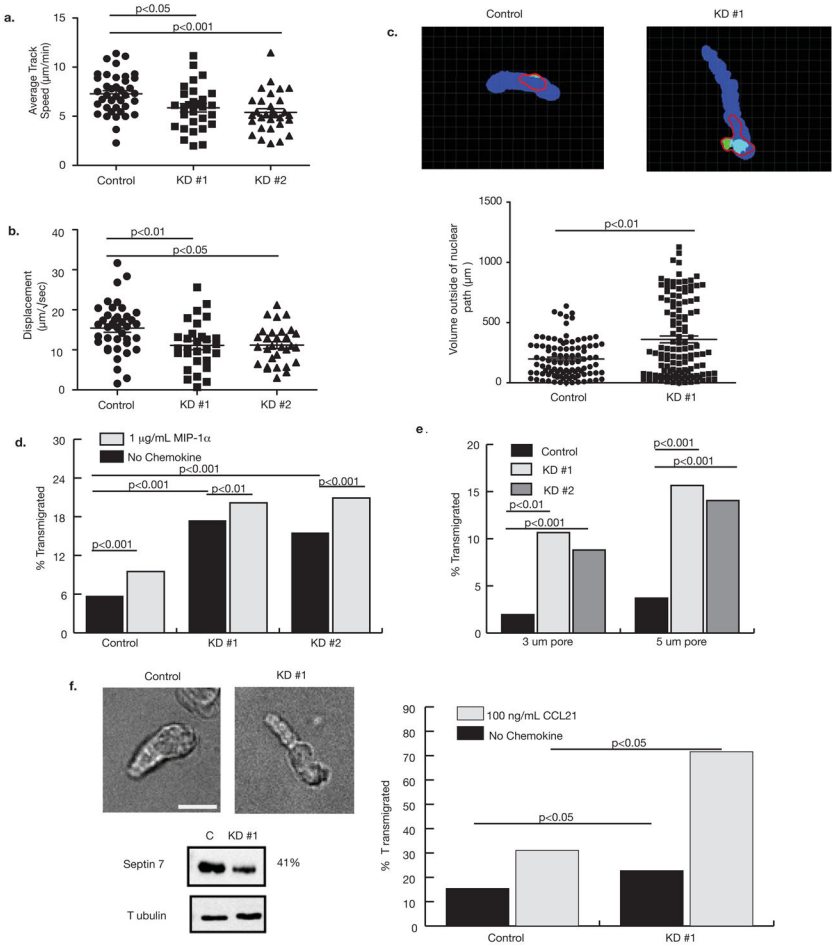

Figure 5. Septins regulate motility and transmigration

(**a**) Overall crawling velocity and (**b**) displacement over time were reduced by Sept7KD. KD #1, n = 31, KD #2, n = 29 and control treated cells n = 39. Similar results were obtained in three independent experiments. Statistical analysis was performed using Kruskal-Wallis tests with Dunn's post-tests. (**c**) Top panels show representative frames from analysis of extra-nuclear path volume. The path of the nucleus over the entire time course is shown in blue. Measured cell body volume deviating from that path is represented in green. The red line shows the outline of the entire cell volume, for reference. The bottom panel shows analysis of multiple time points for at least 10 different cells and a Mann-Whitney U test indicates that Sept7KD cells make significantly more protrusions out of the direction of motility than control cells. (**d**) Responsiveness of control and Sept7KD T cells to MIP-1α chemokine gradients in a transwell assay using 8μm pores. Both control and Sept7KD cells had weak migration to the chemokine, but Sept7KD cells passed through the pores approximately 2-fold better than control cells. (**e**) Sept7KD T cells transmigrate through extremely small pores whereas control cells are constrained from passage. Transmigration (in the absence of chemokine) was assessed using transwells with 3 μm and 5 μm pores. Similar results were obtained in three independent experiments. (**f**) Sept7KD DO11.10 T cell blasts show a similar extended-uropod phenotype to Sept7KD D10 cells. Scale bar represents 10 μm. (**e**) Sept7KD DO11.10 cells transmigrate more efficiently in response to

CCL21 than control cells. Transwell inserts with 5 μm pores were used in these assays. Data shown is representative of two experiments.

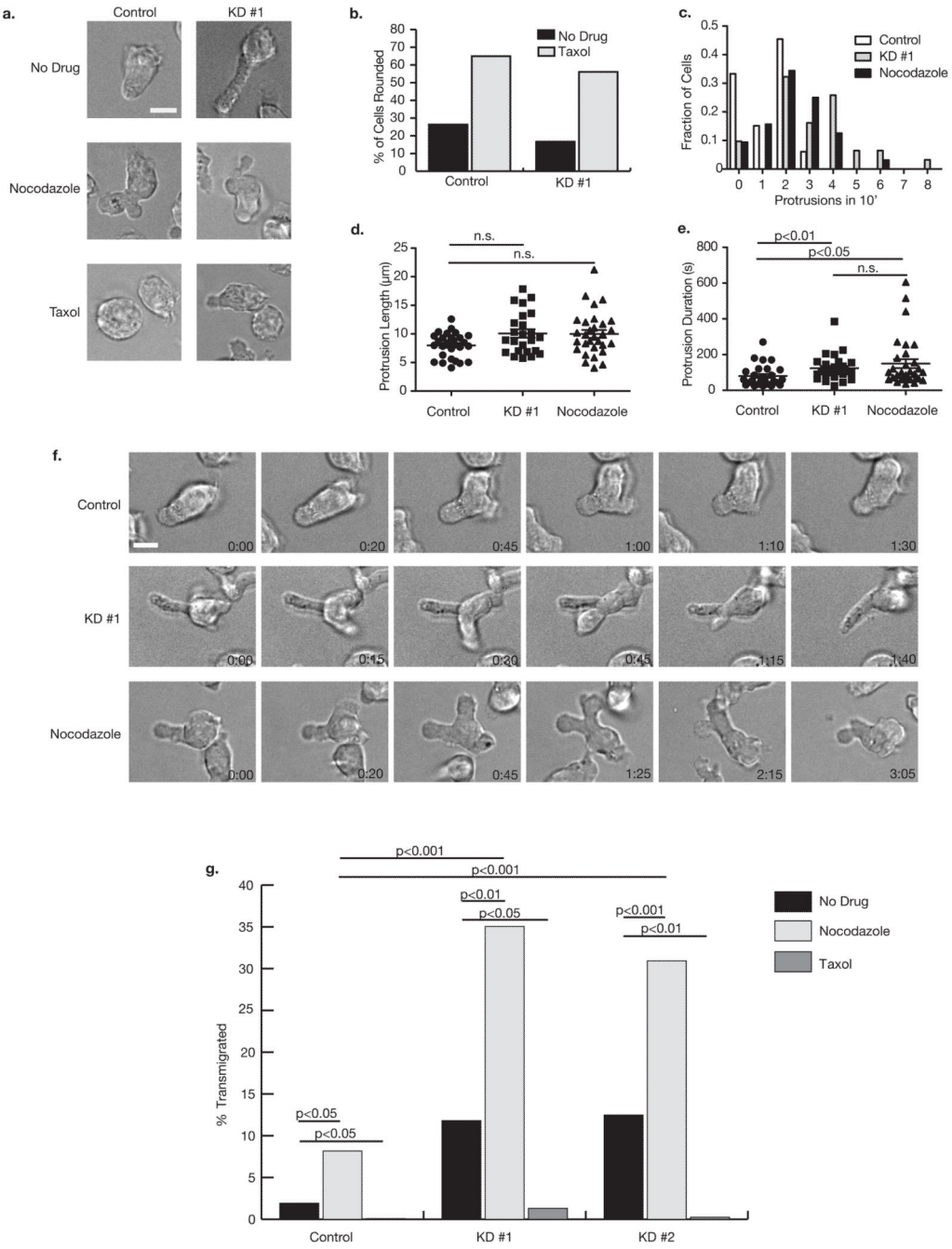

Figure 6. Septins and microtubules regulate rigidity and transmigration

(**a**) Images of control or Sept7KD D10 were taken after treatment with no drug, 5 μM nocodazole or 5 μM taxol for at least 30 minutes. (**b**) Taxol treatment caused both Sept7KD and control cells to become rounded implying a dependence of the Sept7KD phenotype on microtubule function. (**c**) Septin depletion and nocodazole treatment both caused an increase in the number of protrusions made by cells in a 10-minute observation period. Analysis represents greater than 30 cells per group. Duration of protrusions (**e**) but not protrusion length (**d**) was significantly increased in both Sept7KD and nocodazole-treated cells relative

to control cells. Analysis in (**d**) and (**e**) is of the first protrusion observed in each cell from (**c**), and was done using the Kruskal-Wallis test with Dunn's post-test (**f**) Representative time lapse images of protrusions observed in control, Sept7KD, and nocodazole-treated cells. (**g**) Nocodazole caused chemokine-independent transmigration of D10 cells through 3 μm pores similar to, and synergizing with, that observed in Sept7KD cells. This nonspecific transmigration was completely abolished by taxol treatment. Cells were treated with drugs for 30 min prior to the beginning of the four-hour assay. Data shown is representative of two independent experiments. Scale bars represent 10 μm.